Semiconductor-based photodiodes with Ni and Zn-centered nicotinates interfacial layers

Abdulkerim Karabulut[1,*], M. Unlu[2], M. Yıldırım[3], D. A. Köse[4], M. O. Erdal[5], and D. E. Yıldız[6,*]

[1] *Department of Basic Sciences, Faculty of Sciences, Erzurum Technical University, Erzurum, Turkey*

[2] *Department of Polymer Science and Technology, Hitit University, 19030 Corum, Turkey*

[3] *Department of Biotechnology, Faculty of Science, Selcuk University, 42130 Konya, Turkey*

[4] *Department of Chemistry, Faculty of Arts and Sciences, Hitit University, 19030 Corum, Turkey*

[5] *Meram Vocational School, Necmettin Erbakan University, 42090 Konya, Turkey*

[6] *Department of Physics, Faculty of Arts and Sciences, Hitit University, 19030 Corum, Turkey*

ABSTRACT

In order to fabricate the semiconductor-based photodetectors, Ni and Zn-centered nicotinate complexes were synthesized chemically. The synthesized Ni and Zn-centered nicotinates were analyzed using Ultraviolet–Visible (UV–Vis) spectrometry and thermogravimetric analysis (TGA) techniques. The synthesized complex materials were coated between Al and p-Si by spin coating technique, and Al/Ni-centered nicotinate/p-Si and Al/Zn-centered nicotinate /p-Si sandwich structures were obtained. The photoelectrical characteristics of the produced devices were analyzed by photo-transient (I-t) and current–voltage (I–V) measurements under dark and different luminous power intensities. In light of the measurements made, series resistance, ideality factor, and barrier height values, which are very important electrical parameters, were obtained and evaluated in particular using different techniques. Various parameters such as specific detectivity, responsivity, and photosensitivity were calculated using I-t analysis based on exposed light power. In addition, external quantum efficiency (EQE) values were calculated with I-t measurements carried out under lighting conditions at different wavelengths. Last of all, the Al/Ni-centered nicotinate/p-Si and Al/Zn-centered nicotinate/p-Si structures have good performance in photodetector and photodiode designs and can be developed for use in optoelectronic technologies.

1 Introduction

Semiconductor/metal structures are of great attention as they can be used in long-lived electronic systems such as capacitors, transistors, solar cells, and diodes [1–4]. While these structures restrict the mobility of the charge carriers when a reverse bias is applied, on the contrary, they provide transmission in the case of positive bias, thus revealing the rectification and switching functions in a healthy way [5–7]. In addition, since polarization occurs, they are considered a capacitor where the charge, hence the energy, can be

Scheme 1 Synthesis reaction scheme of metal cation-nicotinate salts
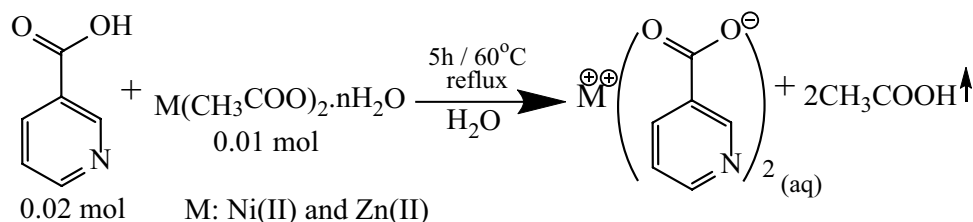
stored. A structure that can be produced must first be suitable for the purpose, that is, it must contain the desired features. One of the most beneficial ways to optimize the desired properties is to coat an inorganic or organic film between the semiconductor and the metal [8–10]. Among the materials that can be used, polymeric structures have inspired many researchers because they are more easily optimized due to the doping of metals [11, 12].

The created structures having interfacial layers form the basis of electronic devices used in every field of technology such as photodetectors, sensors, solar cells, and photodiodes. Photodiodes, which differ in their intended use from solar cells, which is one of the important photovoltaic devices, focus on the perception of signals and their sensitivity to stimuli and have come a long way with the developing materials perspective and new technological developments [13]. The photoelectric effect, which can be defined as the inclusion of electrons in the system as a result of the electron detachment of photons with sufficient energy by hitting the target material, is the basic principle for photodiodes [14–16]. Therefore, the key parameter for photodiodes is the resulting current values in illumination and dark conditions. In this study, complexes with Ni and Zn transition metals in the center were synthesized. Transition metals are intensely preferred in technology to keep the device stable due to their properties such as hardness, high melting and boiling points and density. However, they are also known to be highly electropositive. The issue that makes such complexes prominent is the mobility of electrons, which consist of organic ligands that donate electrons to the central cation.

The method to be used for coating such materials to the desired surface, which is the semiconductor surface in this study, is very important. There are different techniques that can be used in this regard, and there may be points where these techniques are superior to each other. The technique used in this study is the spin coating method and its very important properties can

be listed as follows: homogeneity, distinctive material blend, excellent control, and low cost [17, 18]. However, ease of application and application conditions are also the most important reasons for preference in coating organic material-based compounds.

In this study, metal-centered complexes, which have an important place in optoelectronic technology, which has shown significant developments, and allow the development of materials with desired properties, were synthesized and used to produce semiconductor-based photodiodes. Related materials were produced for the first time and the obtained results were presented comparatively. It is thought that the prepared devices within the scope of the study can be developed for optoelectronic technology, and thus it is concluded that they can be used in different optoelectronic applications.

2 Experimental details

2.1 Synthesis of materials

The reagents utilized in the synthesis of transition metal complexes nicotinic acid ($C_6H_5NO_2$), N, N-diethylnicotinamide ($C_{10}H_{14}N_2O$), zinc acetate ($Zn(CH_3COO)_2 \cdot 2H_2O$) and Nickel acetate ($Ni(CH_3COO)_2 \cdot 4H_2O$) were purchased from Sigma-Aldrich. Synthesis reactions were carried out in deionized solvent.

The metallic nicotinate salts were prepared by separately reacting acetate salts of metal cations with nicotinic acid in aqueous solution (Scheme 1). The stoichiometric molar ratios of the metal cation and nicotinic acid were set to 1:2. 0.01 mol of nickel acetate (2.488 g) or zinc acetate (2.195 g) salts were added to 0.02 mol (2.462 g) nicotinic acid dissolved in deionized water of 100 mL. When completely clear solutions were formed, 0.02 mol of N,N-diethylnicotinamide (3.565 g) was added to each metal-nicotinate solution (Scheme 2). The total reaction solutions formed

Scheme 2 The reaction scheme of Ni(II) and Zn(II) metal cation centered nicotinate/N,N-diethylnicotinamide mixed ligand complex during the synthesis phase

M: Ni(II) and Zn(II)
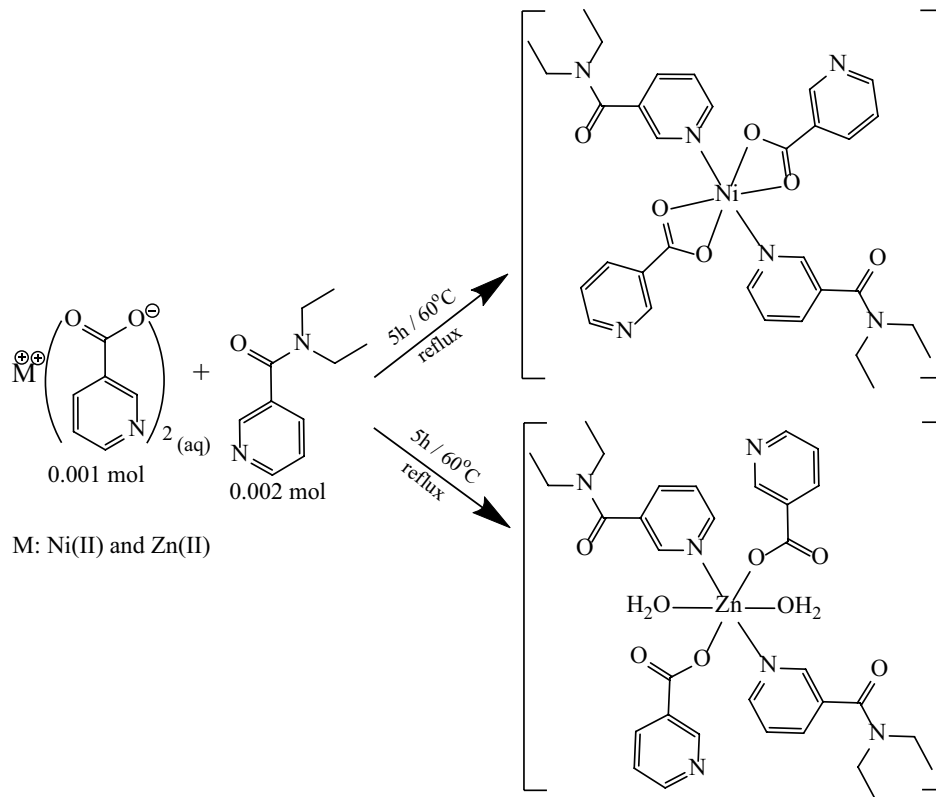
were mixed on a magnetic mixer hot-plate at 60 °C for about five hours [19, 20]. The beakers into which the final solutions were transferred were closed with perforated paraffin film and kept at room temperature until crystal creation. After 20–25 days, the complexes of metal cations were collected as brilliant green crystals for Ni(II) and white for Zn(II).

2.2 Fabrication of photodiodes

In the study, p-type silicon was used as the base material and the properties of the used silicon can be listed as follows: 7.3×10^{15} cm^3 carrier concentration, (100) crystal orientation, one side polished. The substrate, which was cut into small pieces before fabrication, was subjected to an ultrasonic bath with acetone, isopropanol and deionized water for 5 min, respectively, for chemical cleaning. Immediately after this process, it was kept in HF:H$_2$O (1:9) mixture for a short time in order to strip the natural oxide layer, which may have formed on the dried substrate material, and immediately rinsed with deionized water and dried with the help of nitrogen gas. The substrates, whose cleaning process was completed, were placed in the thermal evaporation unit for making ohmic contact and coated

with approximately 80 nm of aluminum metal under appropriate pressure conditions and annealed at 450 °C for 4.5 min under argon gas flow to prevent oxidation. Then, the synthesized metallic complexes were coated on each semiconductor substrate (with ohmic contact) by spin coating technique, and the coating process was carried out at 3000 rpm for 20 s, and the coated pieces were placed on a hot plate and heated at 80 °C for 1 h. After this process, the rectifying metal contacts were obtained using the shadow mask, which consists of a series of circles with a diameter of 1 mm, with the help of thermal evaporation technique. In this way, the production processes of Al/Ni and Zn-centered metallic nicotinates/semiconductor devices were completed.

2.3 Materials and methods

The chemical contents of the complexes were determined with the Korloerva 1106 model elemental analyzer. In addition, the device used to perform TGA analysis is the Shimadzu TG60H. The Shimadzu UV-3600i Plus UV–Vis-NIR Spectrophotometer was utilized for UV–Vis spectrometer measurements. Photoelectrical measurements were performed using the

Fytronix FY-7000 instrument. A home-brewed light-emitting diode (LED) system was utilized for measurements with light of different wavelengths.

3 Results and discussion

3.1 Structural properties

The proposed molecular formulas for the synthesized complex compounds were also supported by chemical composition analyses. The theoretical and experimental elemental analysis results of the compounds agree with each other. For the Ni(II) complex ($C_{32}H_{36}N_6NiO_6$), experimental, C:58.63%; H:5.97%; N:12.67%, calculated, C:58.29%; H:5.50%; N:12.75%.

For the Zn(II) complex ($C_{32}H_{40}N_6O_8Zn$), experimental, C:54.33%; H:5.18%; N:11.89%, calculated, C:54.74%; H:5.74%; N:11.97%.

The data of the products and degradation steps produced from the thermal analysis curves of the complexes shown in Fig. 1a and b are discussed in Table 1. The differences observed in the thermal analysis curves of the complexes coincide with the structural differences proposed for Ni(II) and Zn(II) metal cation complexes. Two crystal waters present in the Zn(II) structure but not in the Ni(II) complex can be shown as the basic structure difference. Due to the absence of crystalline water in its structure, the metal Ni(II) cation provides its octahedral geometry with the nicotinate ligand, which shows chelate bonding through the carboxylate group (Scheme 2).
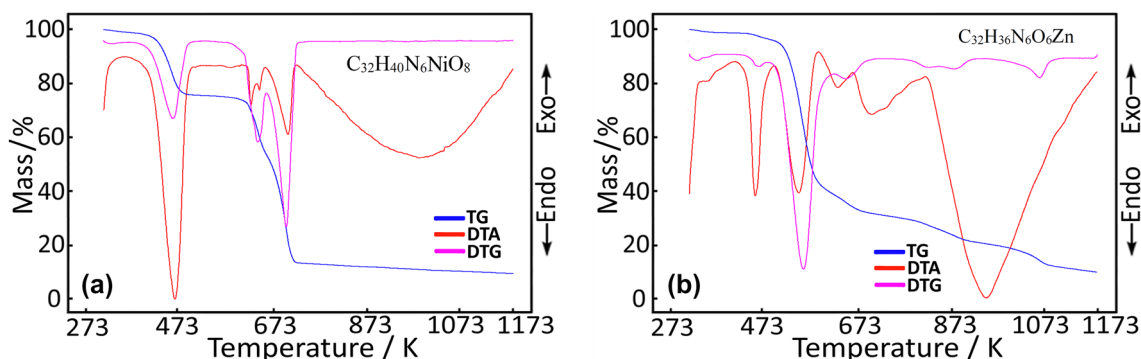

Fig. 1 TG-DTG and DTA curves of the **a** Ni(II) nicotinate complex $[Ni(C_6H_4NO_2)_2(C_{10}H_{14}N_2O)_2]$ and **b** Zn(II) nicotinate complex $[Zn(C_6H_4NO_2)_2(C_{10}H_{14}N_2O)_2(H_2O)_2]$ complexes

Table 1 Thermal analysis data of metal-nicotinate/N,N-diethylnicotinamide mixed ligand complex

Complexes		Temp. range (°C)	DTA$_{max}$(°C)	Removed groups	Mass loss (%)		Remain product (%)		Decomp. product	Color
					Exp.	Calc.	Exp.	Calc.		
$[Ni(C_6H_4NO_2)_2(C_{10}H_{14}N_2O_2)]$										Shine-green
$C_{32}H_{36}N_6NiO_6$	1	40–96	89	$H_2O_{(moisture)}$	1.07	–				
659.37 g/mol	2	115–220	175	$2 N(C_2H_5)_2$	19.69	20.19				
	3	287–373	340,356	$2C_5H_4N$	23.18	23.68				
	4	374–460	416	$C_6H_4NO;CO$	35.97	36.43				
	5	463–877	704	CO_2	5.89	6.68	12.13	11.33	NiO	Black
$[Zn(C_6H_4NO_2)_2(C_{10}H_{14}N_2O)_2(H_2O)_2]$										White
$C_{32}H_{40}N_6O_8Zn$	1	77–226	171	$2H_2O$	5.29	5.12				
702.09 g/mol	2	228–303	264	$2C_{10}H_{14}N_2O$	51.26	50.71				
	3	305–528	345,421	C_6H_4NO	15.06	15.11				
	4	530–862	664,781	$C_6H_4NO_2$	17,77	17,39	12.18	11.59	ZnO	Black

Thermal decomposition of Ni(II) complex, decomposition of organic ligands started and complete decomposition took place in five steps. It has been interpreted as the H_2O removal, which can be described as the first step of moisture water. It was claimed that the two neutrally bound N,N-diethylnicotinamide (*dena*) ligands in the structure were removed in the temperature range of 115–220 °C, with the weight losses of experimental and theoretical being compatible. In the next step, degradation of the pyridine ring of one of the two nicotinate ligands bound to the metal cation as a monoanionic bidentate was interpreted (den. 23.18%; theo. 23.68%). In the fourth step, it was determined that the other nicotinate ligand was broken down. One CO removal with this ligand was also found by weight loss analysis. In the 463–877 °C temperature region, it is claimed that the remaining organic residue is separated from the structure in the form of CO_2 gas. The weight loss (den. 12,13%; theo. 11.33%) and powder XRD analysis confirmed that NiO residue remained in the reaction vessel as the final ruin product of the completely degraded complex structure. The fact that the color of the final residue product was black and the experimental weight loss was approximately 1% higher than the theoretical weight loss was attributed to the precipitation of a part of the incompletely combustible organic residue as carbonized carbon on the metal oxide residue due to insufficient oxygen.

The thermal decomposition of the other Zn(II) metal cation-centered complex took place in four steps and started with the separation of two metal-coordinated crystal waters between the 77–226 °C temperature values (den. 5.29%; theo. 5.12%). It has been referred to the combustion degradation of two dena ligands that coordinated neutrally to the metal between the 228 to 303 °C temperature values (den. 51.26%; teo. 50.71%). In the third and fourth steps, separate degradation of two nicotinate ligands coordinated to the structure as monoanionic monodentate occurred. The fact that the theoretical and experimental weight losses of these steps are compatible with each other also strengthens my claim (Table 1). The residual product of the thermal decomposition of the Zn(II) metal complex was verified by powder XRD analysis to be ZnO. Again, as in the other complex, it accumulated on the non-combustible carbonized carbon oxide residue, causing its color to be black instead of white and the experimental weight loss to be slightly higher than the theoretical weight loss [21].
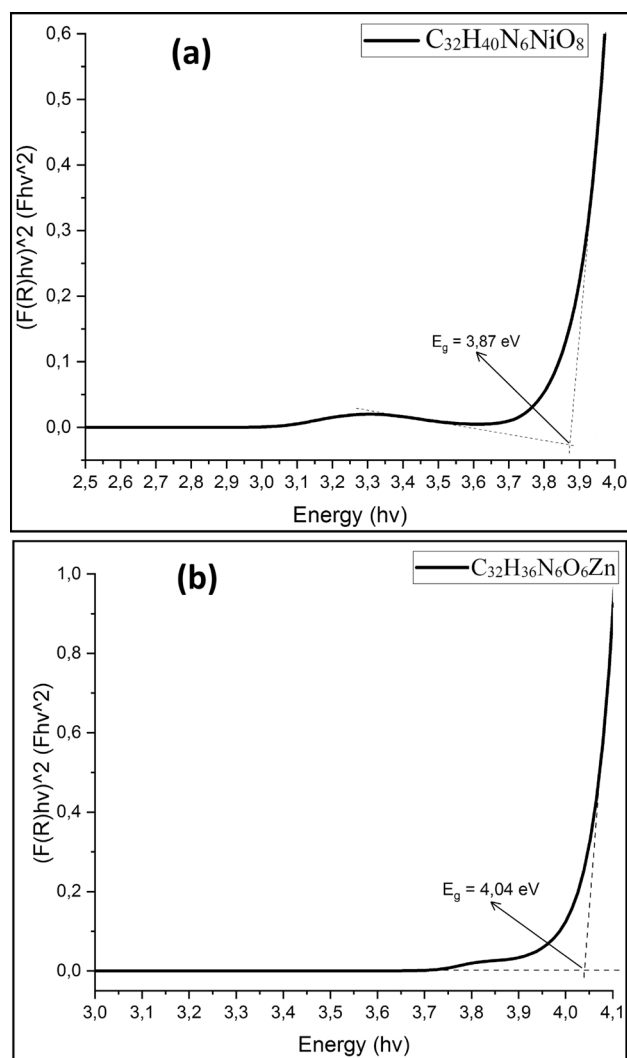

Fig. 2 E_g curves of **a** Ni (II) nicotinate complex and **b** Zn (II) nicotinate complex

The UV–Visible spectrometer was utilized to acquire band gap (E_g) values. Figure 2a and b show the E_g values of the Ni(II) and Zn (II) nicotinates, respectively. The band gap values for Ni(II) and Zn(II) centered complexes were found as 3.87 and 4.04 eV, respectively. These results, which show that the synthesized complexes can be utilized in the production of UV photodetectors, suggest that the complexes are too high to be used in solar cell applications.

3.2 Electrical properties

Figure 3a and b illustrate the I–V properties of Al/Ni-centered nicotinate/p-Si and Al/Zn-centered nicotinate/p-Si diodes for dark and various
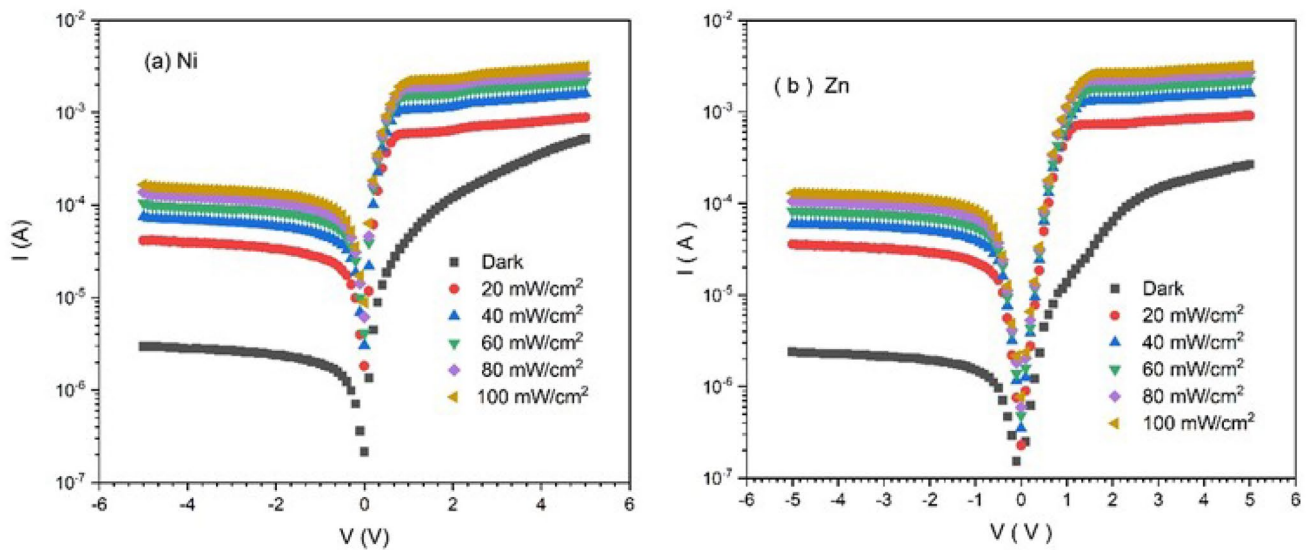
Fig. 3 I–V properties of **a** Al/Ni(II) nicotinate complex/p-Si and **b** Al/ Zn(II) nicotinate complex/p-Si devices

illumination intensities. In the negative bias region, the photoconductive characteristics of the prepared diodes were observed with the increase of the dark current while the illumination was on. It should be noted here that the photocurrent generation leads to an increase in the dark current. In essence, the mentioned photocurrent corresponds to the current of reverse bias. The light hit on the photodiode results in electron–hole pair production in the depletion layer. The produced carriers could straightforwardly cross the barrier. Here, it should be noted that the charge carriers cause a photocurrent under forward bias against the current existing in the diode. It could be safely concluded that the fabricated diode could be used as a photodetector and photodiode.

However, vital electrical parameters like, series resistance (R_s), barrier height (Φ_{Bo}), and ideality factor (n) can be determined with the help of this graph. Thermionic emission theory (TE), in which the current-voltage characteristics of Al/Ni-centered nicotinate/p-Si and Al/Zn-centered nicotinate/p-Si device obey, is used in the calculation of the relevant parameters. According to this theory, the current expression is [22];

$$I = I_L \left[\exp\left(-\frac{q(V - IR_s)}{kT} \right) - 1 \right],$$ (1)

where in I_L is the saturation current and formulaically it is as follows [23];

$$I_L = AA^*T^2 \exp\left(-\frac{q\Phi_b}{kT} \right)$$ (2)

The abbreviations of q, T, ϕ_b, A, k and A^* in relations above stand for the charge, temperature, barrier height, metallic contact area, Boltzmann constant, and Richardson constant (32 A/cm^{-2}K^{-2} for p-type Si), respectively. With the help of the formulaic definitions above, n and ϕ_b can be determined with the following equations [4].

$$n = \frac{q}{kT} \left(\frac{dV}{d(\ln I)} \right)$$ (3)

and,

$$\Phi_b = \frac{kT}{q} \ln \left(\frac{AA^*T^2}{I_L} \right)$$ (4)

Table 2 shows the electrical parameters extracted from the data in Fig. 3a and b. As it is well known, the Φ_{Bo} is decreased while the light intensity increases leading to an increase in the ideality factor. Obtained values of parameters are given visually in Fig. 4a and b for both devices.

As can be seen from the graphs in Fig. 3, the Al/ Ni-centered nicotinate/p-Si and Al/Zn-centered nicotinate/p-Si devices show rectifying behavior, and the rectification ratio value calculated depending on the light intensities is given in Table 2. The rectification ratio decreases as the light intensity increases, as expected. However, when the Ni-centered nicotinate

Table 2 Some electrical parameters for fabricated devices

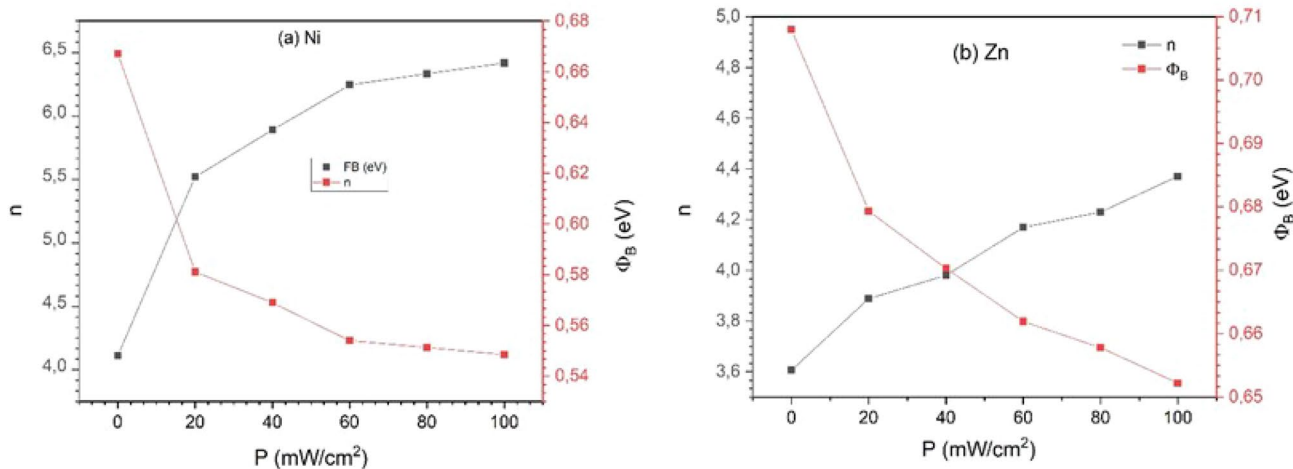|	n	ϕ_b (eV)	RR	R_s (kΩ)		ϕ_b (eV)	
Ni-Complex							
0	4.111	0.667	176.11	dV/dln(I)	H(I)	dV/dln(I)	H(I)
				10.830	11.695	0.792	0.761
20	5.521	0.581	21.41				
40	5.891	0.569	21.34				
60	6.246	0.554	20.74				
80	6.336	0.551	19.31				
100	6.419	0.548	18.93				
Zn-Complex							
0	3.606	0.708	111.65	dV/dln(I)	H(I)	dV/dln(I)	H(I)
				13.164	13.310	0.834	0.796
20	3.888	0.679	25.37				
40	3.980	0.670	26.94				
60	4.169	0.662	26.61				
80	4.230	0.658	25.68				
100	4.370	0.652	24.41				

Fig. 4 Variation of n and ϕ_b values depending on light intensity for **a** Al/ Ni(II) nicotinate complex/p-Si and **b** Al/ Zn(II) nicotinate complex/p-Si devices

and Zn-centered nicotinate complexes are compared, the rectification ratio values of the device produced with the Ni-centered complex are higher in dark conditions. However, when the electrical parameters are evaluated, it is seen that the device having the Ni-centered complex interlayer with a lower ideality factor has better electrical properties. In a study, the ideality factor value for a photodiode produced with indigo material coated between Au and n-Si was found to be 4.39. They reported that the value found was suitable for a device with an interface layer [24].

Karabulut et al. [25] produced a silicon-based photo-detector having a Ruthenium complex interlayer and analyzed the electrical properties of the device they produced. In their study, they obtained the barrier height and ideality factor values as 0.59 eV and 9.42, respectively.

Electrical parameters, which are series resistance and barrier height, could be further determined using Cheung's functions by series resistance means. The method works with the use of the current-voltage values and Fig. 5a and b provide the obtained
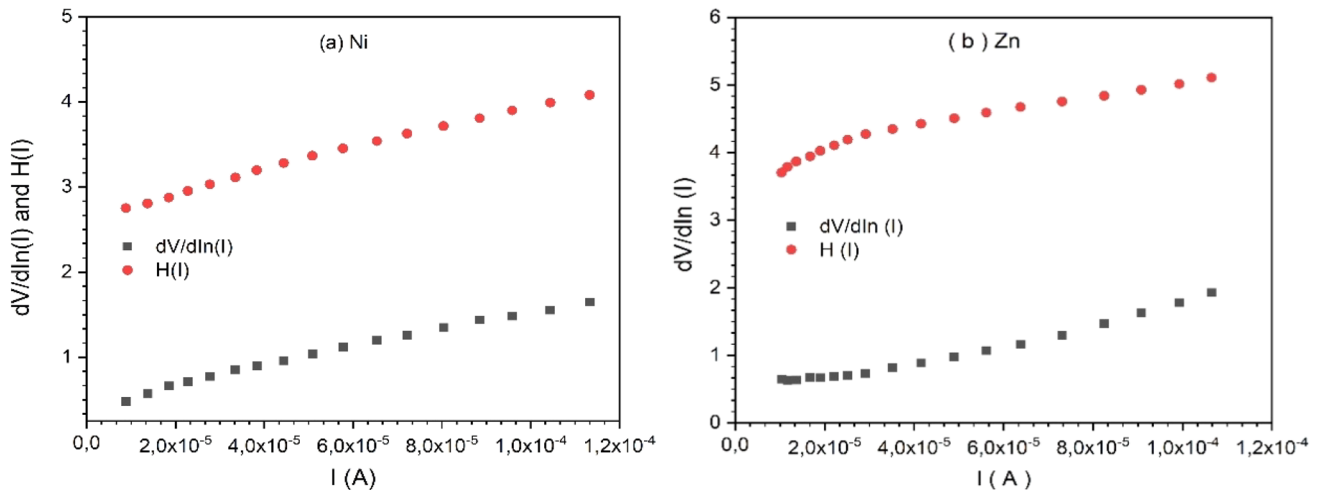
Fig. 5 Cheung graphs of the fabricated devices having **a** Ni(II) nicotinate complex and **b** Zn(II) nicotinate complex interlayers

results for a clearer view. The mentioned Cheung calculations could be provided by the next equations [26];

$$\frac{d(V)}{d(\ln I)} = \frac{nkT}{q} + IR_s \tag{5}$$

And

$$H(I) = n\Phi_b + IR_s \tag{6}$$

Equations 5 and 6 provide $dV/d(\ln I)$ and $H(I)$ values and the numbers are illustrated against the current values in Fig. 6a and b graphs that were drawn for the dark conditions. The obtained curves on

the graphs must be linear since the used equations require the linearity. In this context, the fits made to the current values were yielded instead of the current values obtained in the graphs. Table 1 sums up the R_s values and Φ_b values obtained using means of Cheung's functions. Once the obtained results are compared with the values extracted from thermionic emission, it is seen that there are some differences in the numerical values of the parameters. This difference could be attributed to the differences in the regions for the evaluations. Here, it was also seen that both groups of equations of R_s showed similar behavior under dark conditions, however, the close
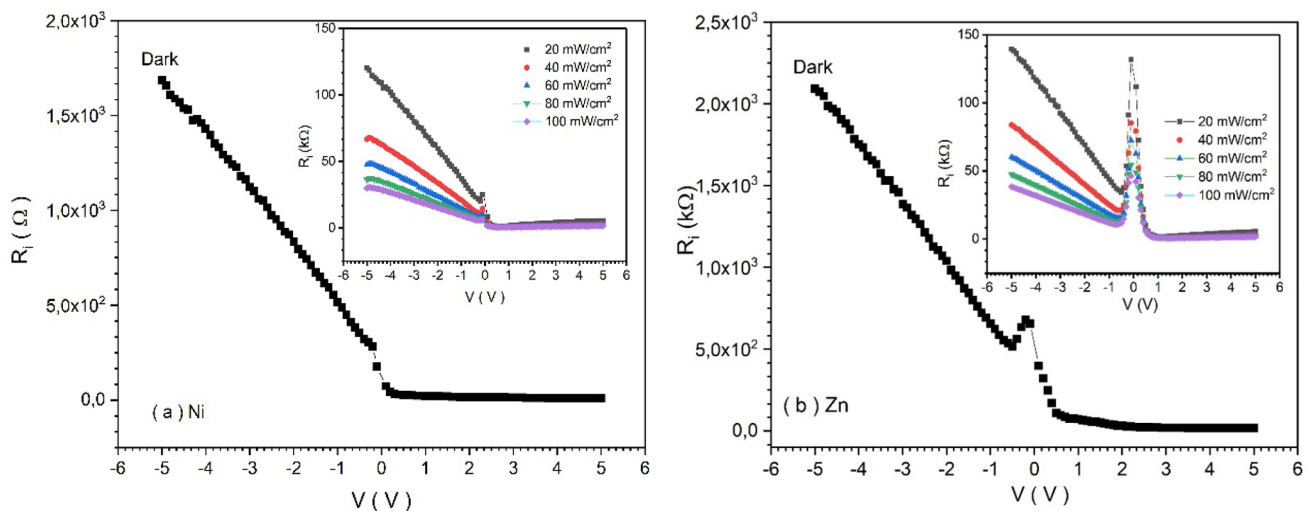

Fig. 6 R_s and R_{sh} versus voltage graphs for the fabricated devices having **a** Ni(II) nicotinate complex and **b** Zn(II) nicotinate complex interlayers

series resistance values for each sample show that the Cheung method works correctly [27].

TE theory with the Gaussian distribution of inhomogeneous barrier height under the impacts of non-ideal behaviors, such as shunt resistance R_{sh} and series resistance R_s, could be helpful to explain the I–V correlation in the reverse and forward regions [28]. It is a known fact that R_s need to be low to reach a good performance of the diode. Here, it should be underlined that the mentioned resistance is related to the interface state effects in the junction, contact regions of diodes, and diode structure. Inhomogeneities on the surface, which can cause localized interface states, and the presence of contacts cause high R_{sh} values [29]. Figure 6a and b of the presented work show the illumination-dependent variation in the value of R_i ($R_i = \partial V/\partial I$) for fabricated devices having Ni-centered nicotinate and Zn-centered nicotinate-based complexes interlayer for all bias voltage spectrums. Besides, a strong illumination dependency exit was observed, and it was found that voltage increase leads to resistance decrease. As can be seen from Table 3, the increase in light intensity has a decreasing effect on parasitic resistance in both regions (positive and negative voltage regions). The resistance decrease occurs due to the fact that illumination increase causes the de-trapping of charges on both sides of bias regions or the number of bonds breaking [30]. Also, the value of resistance variation with voltage is shown in the figures. A sensitivity of series and shunt resistances to the applied voltage and light intensity could be concluded in Fig. 6a and b; Table 3.

Another important issue to be learned for photodetectors and photodiodes is the elucidation of the photoconductivity mechanism. To evaluate this

situation, it is necessary to draw a graph of photocurrent against light intensity. In this context, the graph of ln (P) versus ln (I_{ph}) was drawn (Fig. 7) and the graph was interpreted using the equation given below [31].

$$I_{Ph} = GP^m, \tag{7}$$

where G, m, P, and I_{ph} could be defined as a constant, an exponent, intensity of light, and photocurrent, respectively. The term used to evaluate the photoconductivity mechanism is the value of m, and it was found to be 0.811 and 0.902 for devices with Ni-centered nicotinate and Zn-centered nicotinate complex interfacial layers, respectively. The value of m found is less than 1, meaning that the localized trap levels show a continuous dispersion [32]. Gozeh et al. [32] used the Cd and La-doped ZnO film grown on silicon as the interfacial layer and produced a photodetector. In the mentioned study, they found the m value to be 0.93. In another study, the m value was obtained as 0.49 for a photodiode produced using GaFeO$_3$ material as interlayer [33]. On the other hand, if the relevant value is higher than 1, it represents that the localized interface states are uniformly distributed over the mobility gap [34].

In order to conduct a proper discussion on the photoresponse characteristics of the prepared diodes, the transient photocurrent values were measured at different intensities of light varying from 20 to 100 mW/cm^2, and Fig. 8 shows the obtained values. It is found that turning on the light causes a rapid current

Table 3 R_s and R_{sh} values under various illumination conditions for fabricated devices

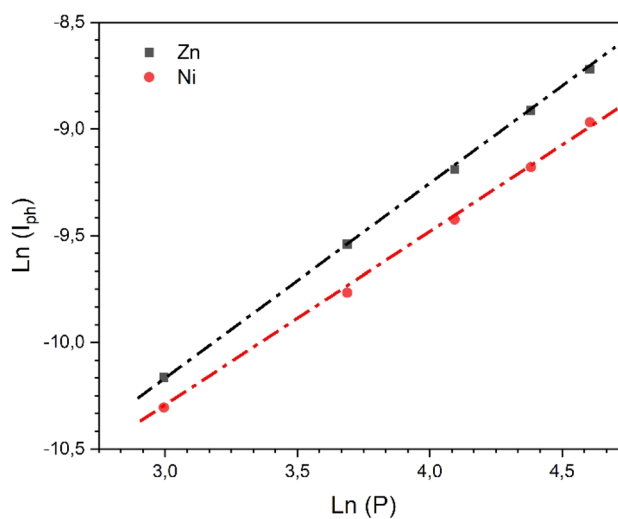|	Ni-complex		Zn-complex	
	R_{sh} (kΩ)	R_s (kΩ)	R_{sh} (kΩ)	R_s (kΩ)
	− 5 V	5 V	− 5 V	5 V
Dark	1686.932	9.579	2092.147	18.738
20 mW/cm^2	120.495	5.628	139.477	5.498
40 mW/cm^2	66.724	3.127	83.764	3.109
60 mW/cm^2	47.578	2.294	60.147	2.260
80 mW/cm^2	36.355	1.883	47.379	1.845
100 mW/cm^2	30.069	1.589	38.537	1.579

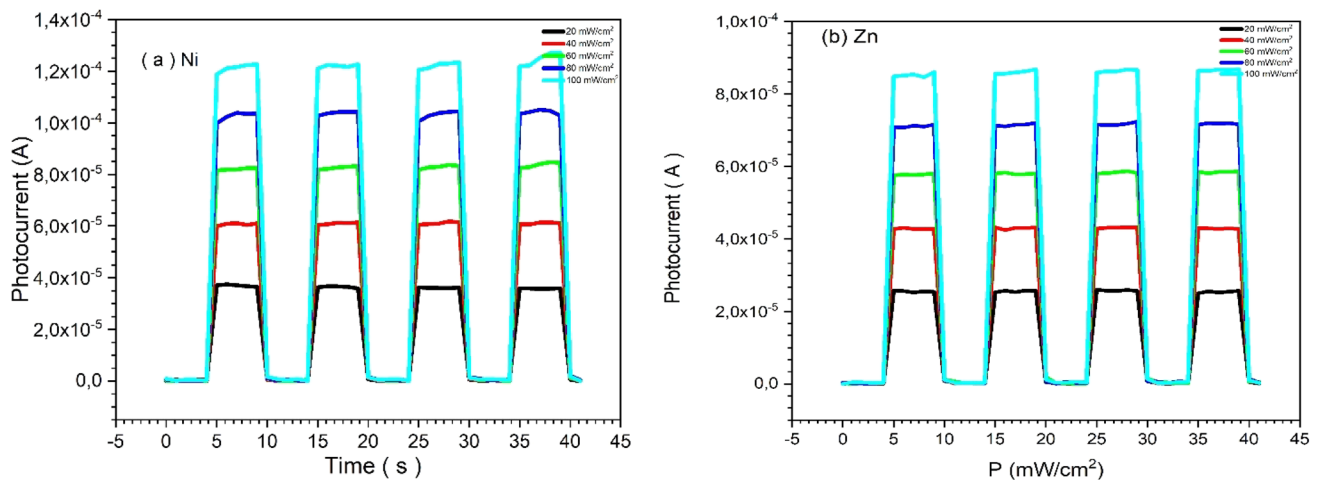**Fig. 7** ln (I_{ph}) versus ln (P) plots for fabricated devices

Fig. 8 Transient photocurrent measurements under different illumination conditions for the fabricated devices having **a** Ni(II) nicotinate complex and **b** Zn(II) nicotinate complex interlayers

increase to a certain level and also gradually to the maximum value. Once the mode is turned off, the photocurrent turns back to the initial value, and that is valid for all fabricated diodes.

The I_{on}/I_{off} ratios, which express the photoresponse performances, were calculated for both devices and it was found that the device with the Ni-centered interlayer had a higher ratio than the Zn-centered nicotinate one. Right after the light strikes the photodiode, the photogenerated charge carriers increase, and electrons support the occurring current. On the other hand, right after the illumination is off, the current and free electrons on the photodiode are decreased. The photoconductive properties of the fabricated devices were related to the trap stations in the metal-centered nicotinate complexes [32]. The occurred current varies with the pass of light states from on to off. In essence, this is due to the fact that the carriers are snared in the deep levels [13]. The fall and rise times of the current with the illumination states should be further determined and could be obtained using a digital oscilloscope. The rise (fall) times were found to be 0.048 (0.037) s and 0.057 (0.043) s for devices having Ni-centered nicotinate and Zn-centered nicotinate materials interlayer, respectively. Additionally, I_{on} and I_{off} processes were performed in 12 and 1 s, respectively.

Another important research carried out in this study is the examination of the effects of wavelength on photocurrent. In Fig. 9, the photocurrent response of the device exposed to light at different wavelengths is given according to time. When the figure is examined, it is seen that as the wavelength increases, the photocurrent value increases in general, but this increase is not regular. The reason for this is attributable to the varying intensity of the effects of trap levels and the surface states [35].

The responsivity (R_p), specific detectivity (D^*) and photocurrent (I_{ph}) values, which are very important detector parameters, can be determined with the help of transient current measurements. In this context, the relevant parameters were calculated for the devices generated with Ni-centered nicotinate and Zn-centered nicotinate interlayers using the equations presented below [5, 36, 37].

$$I_{ph} = I_{illumination} - I_{dark} \tag{8}$$

$$R_P = \frac{I_{ph}}{PA} \tag{9}$$

And

$$D^* = R_P \sqrt{\frac{A}{2qI_{dark}}} \tag{10}$$

In the above formulaic expressions, the abbreviations A and P define the active detector area and the incident light power density, respectively.

The variation of the responsivity and detectivity values depending on the light intensity were presented in Fig. 10a and b, respectively, and also the values of the relevant parameters were yielded in Table 4.
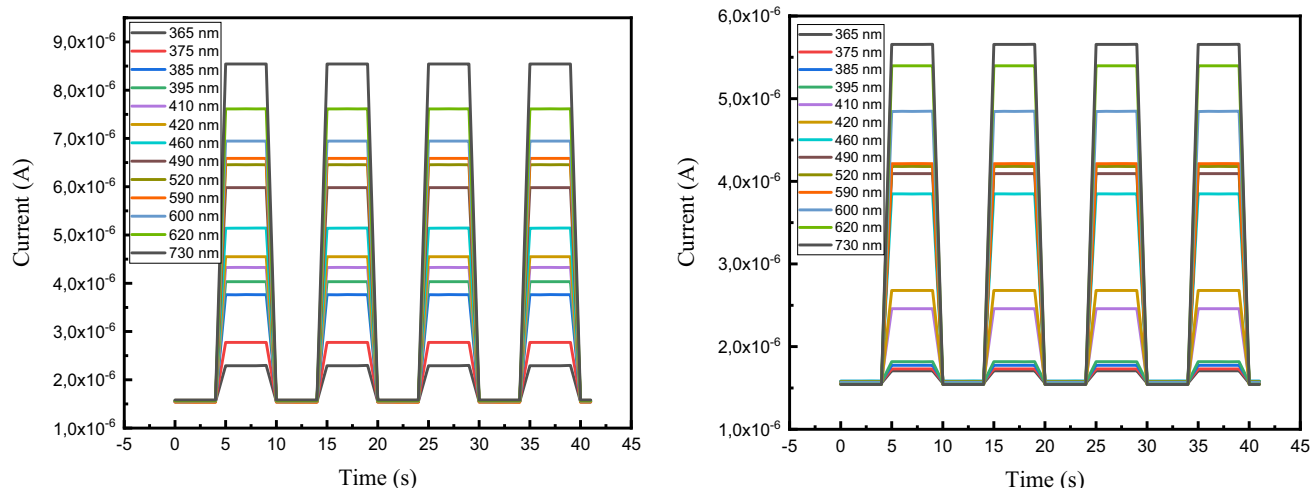
Fig. 9 Transient photocurrent measurements for fabricated devices with **a** Ni(II) nicotinate complex and **b** Zn(II) nicotinate complex interlayers exposed to light at different wavelengths
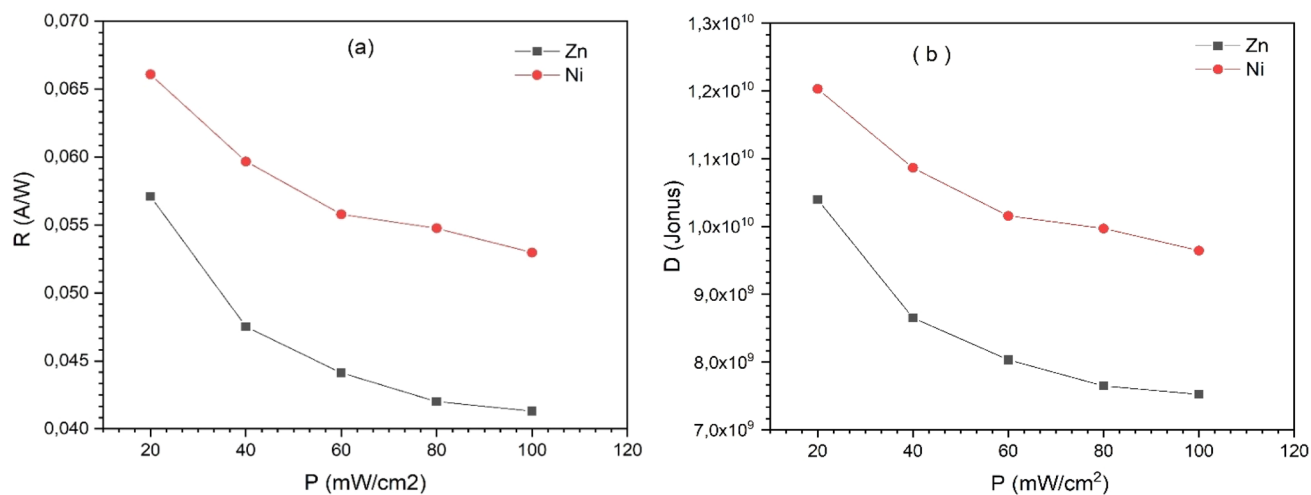

Fig. 10 **a** Responsivity and **b** detectivity versus power intensity graphs of fabricated devices

This situation can be attributed to more trapping of mobility charges due to the rise in interfacial traps due to the material used. It is seen that the I_{ph} values for both devices show an almost linear increase in parallel with the increase in the light intensity, which can be expressed as the increase in the number of charge carriers in the depletion regions with the increase in the light intensity hitting the device. Another value calculated in the study is the external quantum efficiency (EQE) value which was obtained using the formula below [35].

$$\text{EQE} = R\frac{hc}{q\lambda_{\text{nm}}} \tag{11}$$

The EQE value is the most important parameter affecting the gathering efficiency of photocarriers and stands for the number of electrons flowing into the circuit resulting from each photon interacting with the device [35, 38]. The EQE values of the devices with complex interface layers, based on Ni and Zn, were calculated for the different wavelength illuminations applied and given in Table 5. The external quantum efficiency (EQE) profiles of the fabricated devices are given in Fig. 11. Calculated values of Zn-Complex and

Table 4 Some detector parameters for fabricated devices depend on the light intensity

	I_{ph}	R	D
Zn-Complex			
20	3.35×10^{-5}	5.33×10^{-2}	1.08×10^{10}
40	5.73×10^{-5}	4.56×10^{-2}	9.24×10^{9}
60	8.07×10^{-5}	4.29×10^{-2}	8.68×10^{9}
80	1.03×10^{-4}	4.11×10^{-2}	8.32×10^{9}
100	1.27×10^{-4}	4.06×10^{-2}	8.22×10^{9}
Ni-Complex			
20	4.15×10^{-5}	6.61×10^{-2}	1.20×10^{10}
40	7.49×10^{-5}	5.97×10^{-2}	1.09×10^{10}
60	1.05×10^{-4}	5.58×10^{-2}	1.02×10^{10}
80	1.38×10^{-4}	5.48×10^{-2}	9.97×10^{9}
100	1.66×10^{-4}	5.30×10^{-2}	9.64×10^{9}
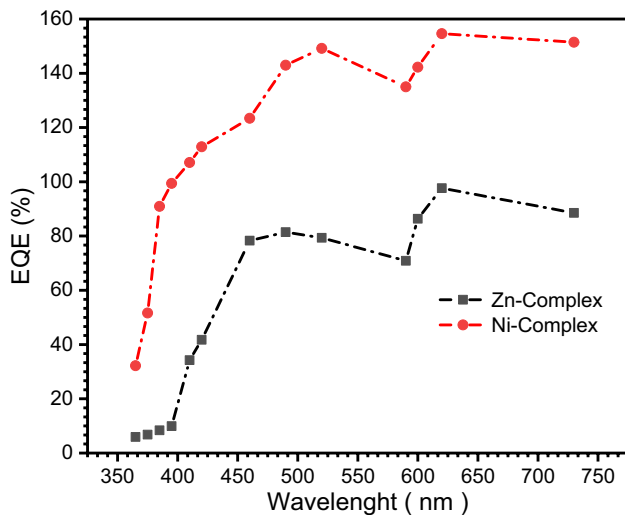
Fig. 11 The external quantum efficiency (EQE) profiles of the fabricated devices

Ni-Complex were found in the range of 5.94–88.33% and 32.18–151.45%. EQE values can exceed 100% due to reasons such as tunneling of the barrier by carriers or excitation of more than one electron by a photon at the interface of the produced Schottky devices [39]. At

wavelengths above 400 nm, the EQE is above 100%, which includes almost the entire visible region. This shows that the produced device can be used as a photodetector for the visible region.

4 Conclusions

Ni-centered nicotinate and Zn-centered nicotinate complexes were synthesized with the help of chemical processes and used as interfacial layers in the production of semiconductor-based Al/Ni-centered nicotinate/p-Si and Al/Zn-centered nicotinate p-Si Schottky photodiodes. By means of TGA analysis of synthesized organic complex materials, mass losses depending on temperature were examined and the content of the material was verified. However, band gap values, which are one of the important optical properties, were determined as 3.87 and 4.04 eV for Ni-centered nicotinate and Zn-centered nicotinate complexes, using UV–Vis spectrometry. The produced photodiodes were electrically characterized by dark and different-intensity light to which they were exposed, and the ideality factor values were found to be 4.11 and 3.66 for Ni-centered nicotinate and Zn-centered nicotinate interfacial layers, respectively, while the barrier height values were calculated as 0.67 and 0.71 eV. However, while testing the relevant values using the Cheung approach, the value of the series resistance and its effects on the devices are discussed. In addition, transient photocurrent measurements were performed for both different light intensities and different wavelengths, and important detector parameters were obtained. The values obtained for the investigated parameters are considered to be sufficient for Schottky devices. The data obtained as a result of the experimental studies indicate that the generated devices have good performance in photodetector and photodiode designs and can be improved for usage in optoelectronic technologies.

Table 5 Some detector parameters for fabricated devices depend on the different wavelength illuminations

	I_{ph}	K	R	D	EQE
Ni-Complex					
365 nm	7.43×10^{-7}	0.48	9.46×10^{-4}	1.19×10^{8}	3.218×10^{-3}
375 nm	1.22×10^{-6}	0.79	1.56×10^{-3}	1.96×10^{8}	5.164×10^{-3}
385 nm	2.21×10^{-6}	1.43	2.82×10^{-3}	3.55×10^{8}	9.095×10^{-3}
395 nm	2.48×10^{-6}	1.60	3.16×10^{-3}	3.98×10^{8}	9.939×10^{-3}
410 nm	2.78×10^{-6}	1.79	3.54×10^{-3}	4.45×10^{8}	1.071×10^{-2}
420 nm	3.00×10^{-6}	1.94	3.82×10^{-3}	4.81×10^{8}	1.129×10^{-2}
460 nm	3.59×10^{-6}	2.32	4.57×10^{-3}	5.75×10^{8}	1.234×10^{-2}
490 nm	4.43×10^{-6}	2.86	5.64×10^{-3}	7.10×10^{8}	1.430×10^{-2}
520 nm	4.91×10^{-6}	3.17	6.25×10^{-3}	7.86×10^{8}	1.492×10^{-2}
590 nm	5.04×10^{-6}	3.25	6.42×10^{-3}	8.07×10^{8}	1.350×10^{-2}
600 nm	5.40×10^{-6}	3.48	6.87×10^{-3}	8.65×10^{8}	1.422×10^{-2}
620 nm	6.06×10^{-6}	3.91	7.72×10^{-3}	9.72×10^{8}	1.546×10^{-2}
730 nm	6.99×10^{-6}	4.51	8.91×10^{-3}	1.12×10^{9}	1.515×10^{-2}
Zn-Complex					
365 nm	1.37×10^{-7}	0.09	1.75×10^{-4}	2.19×10^{7}	5.95×10^{-4}
375 nm	1.61×10^{-7}	0.10	2.05×10^{-4}	2.56×10^{7}	6.78×10^{-4}
385 nm	2.04×10^{-7}	0.13	2.60×10^{-4}	3.25×10^{7}	8.38×10^{-4}
395 nm	2.47×10^{-7}	0.16	3.15×10^{-4}	3.94×10^{7}	9.90×10^{-4}
410 nm	8.88×10^{-7}	0.57	1.13×10^{-3}	1.41×10^{8}	3.42×10^{-3}
420 nm	1.11×10^{-6}	0.71	1.41×10^{-3}	1.77×10^{8}	4.18×10^{-3}
460 nm	2.28×10^{-6}	1.45	2.90×10^{-3}	3.63×10^{8}	7.83×10^{-3}
490 nm	2.52×10^{-6}	1.61	3.21×10^{-3}	4.02×10^{8}	8.14×10^{-3}
520 nm	2.61×10^{-6}	1.66	3.32×10^{-3}	4.15×10^{8}	7.93×10^{-3}
590 nm	2.64×10^{-6}	1.68	3.37×10^{-3}	4.21×10^{8}	7.09×10^{-3}
600 nm	3.28×10^{-6}	2.09	4.18×10^{-3}	5.22×10^{8}	8.64×10^{-3}
620 nm	3.83×10^{-6}	2.44	4.88×10^{-3}	6.10×10^{8}	9.76×10^{-3}
730 nm	4.09×10^{-6}	2.60	5.21×10^{-3}	6.51×10^{8}	8.85×10^{-3}

Author contributions

AK: writing—review & editing, writing—original draft, investigation, supervision. MU: methodology, investigation, writing—original draft. MY: methodology, investigation. DAK: methodology, investigation. MOE: investigation. DEY: writing—original draft, investigation, writing—review & editing, investigation, supervision.

Funding

Data availability

The datasets generated during and/or analyzed during the current study are available from the corresponding author on reasonable request.

Declarations

Conflict of interest   The authors declare that they have no known competing financial interests or personal relationships that could have appeared to influence the work reported in this paper.

References

1. M.J. Sung, K. Kim, S.K. Kwon, Y.H. Kim, D.S. Chung, Phenanthro [110,9,8-cdefg] carbazole-thiophene, donor-donor copolymer for narrow band green-selective organic photodiode. J. Phys. Chem. C **121**, 15931–15936 (2017)

2. A. Tombak, Y. Selim, S. Asubay, T. Kilicoglu, Fabrication and electrical properties of an organic–inorganic device based on coumarin 30 dye. Mater. Sci. Semicond. Process. **24**, 187–192 (2014). https://doi.org/10.1016/j.mssp.2014.03.004

3. B.A. Gozeh, A. Karabulut, A. Yildiz, A. Dere, B. Arif, F. Yakuphanoglu, SILAR controlled CdS nanoparticles sensitized CdO diode based photodetectors. Silicon **12**, 1673–1681 (2019). https://doi.org/10.1007/s12633-019-00266-7

4. D.E. Yildiz, H.H. Gullu, A. Sarilmaz, F. Ozel, A. Kocyigit, M. Yildirim, Dark and illuminated electrical characteristics of Si-based photodiode interlayered with CuCo 5 S 8 nanocrystals. J. Mater. Science: Mater. Elect. **31**(2), 935–948 (2020). https://doi.org/10.1007/s10854-019-02603-3

5. A. Karabulut, D.E. Yıldız, D.A. Köse, M. Yıldırım, Photosensing performances of heterojunctions-based photodiodes with novel complex interlayers. Mater. Sci. Semiconduct. Process. **146**, 106647 (2022). https://doi.org/10.1016/j.mssp.2022.106647

6. S. Aydogan, A. Kocyigit, B.B. Cirak, E. Erdogan, M. Yilmaz, The electrical and dielectric characterization of the Co/ZnO-Rods/p-Si heterostructure depending on the frequency. J. Mater. Sci.: Mater. Electron. **33**(9), 6059–6069 (2022). https://doi.org/10.1007/s10854-022-07784-y

7. F. Unal, M.S. Kurt, S. Aktas, M. Kabaer, Synthesis and optoelectronic characterization of coronene/CdO self-powered photodiode. J. Mater. Sci.: Mater. Electron. (2022). https://doi.org/10.1007/s10854-022-09237-y

8. Ö. Sevgili, F. Lafzi, A. Karabulut, I. Orak, S. Bayındır, The synthesis of new bola-amphiphile TPEs and the comparison of current transformer mechanism and structural properties for Al. Compos. Part. B: Eng. **172**, 226–233 (2019). https://doi.org/10.1016/j.compositesb.2019.05.020. /Bis (HCTA)-TPE/p-Si and Al/Bis (HCOA)-TPE/p-Si heterojunctions

9. D.E. Yıldız, H.H. Gullu, H.K. Cavus, Effect of TiO2 Thin Film with different dopants in bringing Au-metal into a contact with n-Si. J. Inorg. Organomet. Polym Mater. **32**(3), 1067–1077 (2022). https://doi.org/10.1007/s10904-021-02201-z

10. E. Özcan, B.T. Aksoy, E.T. Eçik, A. Dere, A. Karabulut, F. Yakuphanoglu, B. Çoşut, Fabrication of hybrid photodiode systems: BODIPY decorated cyclotriphosphazene covalently grafted graphene oxides. Inorg. Chem. Front. **7**(16), 2920–2931 (2020). https://doi.org/10.1039/D0QI00468E

11. A. Kocyigit, M. Yıldırım, D.A. Kose, D.E. Yıldız, Synthesize and characterization of Co-complex as interlayer for Schottky type photodiode. Polym. Bull. (2022). https://doi.org/10.1007/s00289-021-04021-0

12. J. Kim, U. Lee, B.K. Koo, Synthesis and 1D chain crystal structure of zinc(II) terephthalate complex: [Zn(tp)(py)(H2O)]n. Bull. Korean Chem. Soc. **31**, 1743–1746 (2010). https://doi.org/10.5012/bkcs.2010.31.6.1743

13. İ. Orak, A. Karabulut, E. Yiğit, Ö. Sevgili, A. Ruşen, F. Ozel, The diode and photodiode performances of BaZrO3 perovskite-based device under the influence of thermal and light external stimuli. Sens. Actuators A: Phys. **337**, 113413 (2022). https://doi.org/10.1016/j.sna.2022.113413

14. G.P. Smestad, Conversion of heat and light simultaneously using a vacuum photodiode and the thermionic and

photoelectric effects. Sol. Energy Mater. Sol. Cells. **82**(1–2), 227–240 (2004). https://doi.org/10.1016/j.solmat.2004.01.020

15. E. Saloma, S. Alcántara, N. Hernández-Como, J. Villanueva-Cab, M. Chavez, G. Pérez-Luna, J. Alvarado, Photoelectric effect on an Al/SiO2/p-Si Schottky diode structure. Mater. Res. Express. **7**(10), 105902 (2020). https://doi.org/10.1088/2053-1591/abbc40

16. K. Kato, H. Tsuruta, T. Ebe, K. Shinbo, F. Kaneko, T. Wakamatsu, Enhancement of optical absorption and photocurrents in solar cells of Merocyanine Langmuir–Blodgett films utilizing surface plasmon excitations. Mater. Sci. Engineering: C **22**(2), 251–256 (2002). https://doi.org/10.1016/S0928-4931(02)00174-1

17. A. Karabulut, F. Lafzi, S. Bayindir, Ö. Sevgili, I. Orak, The synthesis, current transformer mechanism and structural properties of novel rhodanine-based Al/Bis (Rh)-Ph/p-Si and Al/Bis (Rh)-TPE/p-Si heterojunctions. J. Mol. Struct. **1231**, 129699 (2021). https://doi.org/10.1016/j.molstruc.2020.129699

18. O. Sevgili, S. Canlı, F. Akman, I. Orak, A. Karabulut, N. Yıldırım, Characterization of aluminum 8-hydroxyquinoline microbelts and microdots, and photodiode applications. J. Phys. Chem. Solids. **136**, 109128 (2020). https://doi.org/10.1016/j.jpcs.2019.109128

19. Z.S. Şahin, M. Demir, T. Yıldırım, Ö. Yurdakul, D.A. Köse, Novel mixed ligand complexes of Co(II), ni(II), Cu(II), and zn(II) with 1,10-phenanthroline and acesulfame. Synthesis, structural analysis and hydrogen adsorption study. Int. J. Hydrogen Energy. **46**, 27631–27642 (2021). https://doi.org/10.1016/j.ijhydene.2021.06.026

20. Ö. Yurdakul, Z.S. Şahin, D.A. Köse, O. Şahin, F. Akkurt, Novel monoanionic diphenate-nicotinamide/N,N-diethylnicotinamide complexes of NiII, ZnII. Synthesis, structural investigations and hydrogen adsorption study. J. Mol. Struct. **1218**, 128514 (2020). https://doi.org/10.1016/j.molstruc.2020.128514

21. Ö. Aybirdi, D.A. Köse, H. Necefoğlu, Synthesis of the 4-N,N-dimethylaminobenzoic acid complexes of Mn(II),Co(II), ni(II), and Cu(II). spectroscopic and thermal characterization. Hacettepe J. Biol. Chem. **36**(1), 31–39 (2008)

22. D.E. Yıldız, A. Karabulut, I. Orak, A. Turut, Effect of atomic-layer-deposited HfO 2 thin-film interfacial layer on the electrical properties of Au/Ti/n-GaAs Schottky diode. J. Mater. Science: Mater. Elect. **32**(8), 10209–10223 (2021). https://doi.org/10.1007/s10854-021-05676-1

23. A. Turut, D.E. Yıldız, A. Karabulut, I. Orak, Electrical characteristics of atomic layer deposited Au/Ti/HfO 2/n-GaAs MIS diodes in the wide temperature range. J.

Mater. Sci.: Mater. Electron. **31**(10), 7839–7849 (2020). https://doi.org/10.1007/s10854-020-03322-w

24. M.A. Manthrammel, I.S. Yahia, M. Shkir, S. AlFaify, H.Y. Zahran, V. Ganesh, F. Yakuphanoglu, Novel design and microelectronic analysis of highly stable Au/Indigo/n-Si photodiode for optoelectronic applications. Solid State Sci. **93**, 7–12 (2019). https://doi.org/10.1016/j.solidstatesciences.2019.04.007

25. A. Karabulut, A. Dere, O. Dayan, A.G. Al-Sehemi, Z. Serbetci, A.A. Al-Ghamdi, F. Yakuphanoglu, Silicon based photodetector with Ru (II) complexes organic interlayer. Mater. Sci. Semi Proces. **91**, 422–430 (2019). https://doi.org/10.1016/j.mssp.2018.11.035

26. Z. Çaldıran, A.R. Deniz, F.M. Coşkun, Ş. Aydoğan, A. Yeşildağ, D. Ekinci, I–V–T (current–voltage–temperature) characteristics of the Au/Anthraquinone/p-Si/Al junction device. J. Alloys Compd. **584**, 652–657 (2014). https://doi.org/10.1016/j.jallcom.2013.09.006

27. L.B. Taşyürek, Ş. Aydoğan, M. Sevim, Z. Çaldıran, Synthesis of nickel nanoparticles-deposited strontium titanate nanocubes (Ni-STO) and heterojunction electrical applications over a wide temperature range. Mater. Sci. Engineering: B **274**, 115479 (2021). https://doi.org/10.1016/j.mseb.2021.115479

28. P. Chattopadhyay, The effect of shunt resistance on the electrical characteristics of Schottky barrier diodes. J. Phys. D **29**(3), 823 (1996). https://doi.org/10.1088/0022-3727/29/3/047

29. H.H. Gullu, D.E. Yildiz, Analysis of forward and reverse biased current–voltage characteristics of Al/Al2O3/n-Si Schottky diode with atomic layer deposited Al 2 O 3 thin film interlayer. J. Mater. Science: Mater. Elect. **30**(21), 19383–19393 (2019). https://doi.org/10.1007/s10854-019-02300-1

30. E. Coşkun, H.H. Güllü, İ. Candan, Ö. Bayraklı, M. Parlak, C. Ercelebi, Device behavior of an In/p-Ag (Ga, In) Te2/n-Si/Ag heterojunction diode. Mater. Sci. Semicond. Process. **34**, 138–145 (2015). https://doi.org/10.1016/j.mssp.2015.02.043

31. N. Demirbilek, F. Yakuphanoğlu, M. Kaya, Structural and optical properties of pure ZnO and Al/Cu co-doped ZnO semiconductor thin films and electrical characterization of photodiodes. Mater. Test. **63**(3), 279–285 (2021). https://doi.org/10.1515/mt-2020-0042

32. B.A. Gozeh, A. Karabulut, A. Yildiz, F. Yakuphanoglu, Solar light responsive ZnO nanoparticles adjusted using cd and La Co-dopant photodetector. J. Alloys Compd. **732**, 16–24 (2018). https://doi.org/10.1016/j.jallcom.2017.10.167

33. M. Soylu, M. Cavas, A. Ahmed, Z.H. Al-Ghamdi, F. Cafer, F. El-Tantawy, Yakuphanoglu, Photoelectrical characterization of a new generation diode having GaFe03 interlayer. Solar Energy Mater. Solar Cells. **124**, 180–185 (2014). https://doi.org/10.1016/j.solmat.2014.01.045

34. M. Cavas, A.A.M. Farag, Z.A. Alahmed, F. Yakuphanoglu, Photosensors based on Ni-doped ZnO/p-Si junction prepared by sol-gel method. J. Electroceram. **31**(3), 298–308 (2013). https://doi.org/10.1007/s10832-013-9839-3

35. A. Kocyigit, A.A. Hussaini, M. Yıldırım, D. Kose, D.E. Yıldız, Schottky type photodiodes with organic co-complex and Cd-complex interlayers. Appl. Organomet. Chem. **36**(11), e6879 (2022). https://doi.org/10.1002/aoc.6879

36. Y. Wang, S. Yang, A. Ballesio, M. Parmeggiani, A. Verna, M. Cocuzza, C.F. Pirri, S.L. Marasso, The fabrication of Schottky photodiode by monolayer graphene direct-transfer-on-silicon. J. Appl. Phys. **128**(1), 014501 (2020). https://doi.org/10.1063/5.0004242

37. B. Son, H. Zhou, Y. Lin, K.H. Lee, C.S. Tan, Gourd-shaped hole array germanium (Ge)-on-insulator photodiodes with improved responsivity and specific detectivity at 1,550 nm. Opt. Express. **29**(11), 16520–16533 (2021). https://doi.org/10.1364/OE.422931

38. A. Pierre, I. Deckman, P.B. Lechêne, A.C. Arias, High detectivity all-printed organic photodiodes. Adv. Mater. **27**(41), 6411–6417 (2015). https://doi.org/10.1002/adma.201502238

39. S.J. Dhoble, N.T. Kalyani, B. Vengadaesvaran, A.K. Arof, Energy Mater.: Fundam. Appl. (2023). https://doi.org/10.3390/ma16145068